Synthesis and characterization of hydroxyapatite, fluoride-substituted hydroxyapatite and fluorapatite

M. WEI*, J. H. EVANS
Centre for Rehabilitation Science and Engineering, Queensland University of Technology, Gardens Point Campus, 2 George St, GPO Box 2434, Brisbane, QLD 4001, Australia

T. BOSTROM
Analytical Electron Microscopy Facility, Queensland University of Technology, Gardens Point Campus, 2 George St, GPO Box 2434, Brisbane, QLD 4001, Australia

L. GRØNDAHL
School of Physical and Chemical Sciences, Queensland University of Technology, Gardens Point Campus, 2 George St, GPO Box 2434, Brisbane, QLD 4001, Australia
E-mail: m.wei@ims.uconn.edu

Powders of hydroxyapatite (HA), partially fluoride-substituted hydroxyapatite (fHA), and fluorapatite (FA) were synthesized in house using optimum methods to achieve relatively pure powders. These powders were assessed by the commonly used bulk techniques of X-ray diffraction (XRD), Fourier transform infra-red (FTIR) and FT-Raman spectroscopies, inductively coupled plasma atomic emission spectroscopy (ICP-AES), and F-selective electrode. In addition, the current study has employed transmission electron microscopy (TEM), involving morphological observation, electron diffraction and energy-dispersive X-ray spectrometry (EDX), as an effective analytical technique to evaluate the powders at a microscopic level.

The HA and fHA particles were elongated platelets about 20 × 60 nm in size, while FA particles were over twice this size. Calcination of the HA and fHA powders at 1000 °C for 1 h resulted in increased grain size and crystallinity. The calcined fHA material appeared to possess a crystal structure intermediate between HA and FA, as evidenced by the (3 0 0) peak shift in XRD, as well as by the position of the hydroxyl bands in the FTIR spectra. This result was consistent with electron diffraction of individual particles. Small levels of impurities in some of the powders were identified by EDX and electron diffraction, and the carbonate content was detected by FTIR. The use of TEM in conjunction with the bulk techniques has allowed a more thorough assessment of the apatites, and has enabled the constituents in these closely related apatite powders to be identified.

1. Introduction

It is well known that hydroxyapatite (HA) is the main component of bones and teeth [1]. Due to its excellent bioactivity but poor mechanical properties as a bulk material [1], it has been widely used in non-load bearing situations, such as maxillo-facial and middle ear reconstructions. When OH^- in HA is partially substituted by F^-, fluoride-substituted hydroxyapatite (fHA) is obtained [1]. If the substitution is completed, fluorapatite (FA) is formed. FA is found in dental enamel, and is normally used in dental applications due to its greater mechanical strength.

HA belongs to the hexagonal crystal system, space group $P6_3/m$ [1], with unit cell dimensions $a = 0.9432$ nm and $c = 0.6881$ nm. This group is characterized by a six-fold c-axis perpendicular to three equivalent a-axes at 120° to each other. FA has a very similar atomic structure and belongs to the same space group as HA, differing only in the substitution of fluoride for the hydroxyl groups in the HA structure. Since F^- is smaller than OH^-, the substitution results in a contraction in the a-axis dimensions to 0.9368 nm, but with no change in the c-axis dimension.

X-ray diffraction (XRD), Fourier transform infra-red (FTIR) and Raman spectroscopy have been widely used to characterize apatites, and detailed reflection angle and

* Author to whom all correspondence should be addressed: Department of Metallurgy and Materials Engineering, University of Connecticut, 97 N. Eagleville Road, Box U-136, Storrs, CT 06269-3136, USA

frequency assignments are well known [2, 3]. The XRD patterns of HA and FA are very similar. However, close observation of the (3 0 0) and (0 0 2) X-ray reflections reveals that the (3 0 0) X-ray reflection peak of FA is shifted to a higher 2θ value, while the (0 0 2) reflection peak of FA is not markedly different from that of HA [2]. The vibrational spectroscopic methods give information about the phosphate and hydroxide vibrations, which are very sensitive to substitution within the apatite lattice [3]. FT-Raman spectra are thus used to provide evidence for the identity of the apatite powders. Furthermore, fluoride substitution in HA causes strong variation in the ν_3 phosphate modes [4]. The FTIR spectra give information about the identity of the hydroxy- and FAS [5, 6] as well as the fluoride content in partly fHA [7, 8].

Other techniques for distinguishing HA and FAs have been explored. Braun *et al*. [9] used ^{31}P NMR and ^{19}F NMR to distinguish these two materials. It was found that ^{31}P NMR could reveal differences between different calcium phosphates, but could not differentiate the FA and HA forms. However, the use of ^{19}F permitted these two apatites to be distinguished.

Transmission electron microscopy (TEM) has previously been used to study the structure of synthetic apatites [10–15]. Kleebe *et al*. [12] studied sintered HA by high resolution TEM, and were able to confirm the space group of the material using convergent beam electron diffraction. Ji and Marquis [13] reported that some HA in samples sintered at 1200 °C may convert to α-$Ca_3(PO_4)_2$ when exposed to the beam in the TEM. In contrast Suvorova *et al*. [14] have demonstrated that HA is generally quite stable under the electron beam, and subsequent work using high resolution TEM and electron diffraction showed that HA was highly crystalline at even the smallest particle sizes [15]. TEM has not, however, been employed as a primary technique to systematically characterize the different apatite forms. In the current study, TEM has not only provided morphological information on the powders, but has been used specifically to try to identify the individual apatite phases and possible impurities in the synthesized powders by electron diffraction and energy-dispersive elemental analysis. Some of these constituents, especially when present in small amounts, may not be detected by macroscopic techniques. Results from TEM analyses have been compared to those from bulk characterization methods such as XRD, FTIR and FT-Raman spectroscopy and ICP to provide a more complete characterization of the synthesized materials.

The three forms of apatite, HA, partially substituted fHA, and FA, were synthesized in house. Previous methods of preparing HA have ranged from conventional powder compaction-sintering techniques to wet process [11, 15–17]. For both dry and hydrothermal processes, it is very difficult to eliminate impurities in the system, though for a wet process some impurities can be excluded by dissolving them in the solution. Thus, a wet process was used to synthesize HA based on the following reaction [11, 16]:

$$10Ca(NO_3)_2 + 6(NH_4)_2HPO_4 + 8NH_4OH \rightarrow Ca_{10}(PO_4)_6(OH)_2 + 20NH_4NO_3 + 6H_2O$$

There are numerous methods of producing partially fHA [2, 9, 10, 20] by substituting the OH^- groups in HA by F^-. Okazaki *et al*. [2, 20] have published a series of articles on substituted FA prepared by using HF as the source of F^-. Due to the high toxicity of HF, this method was not employed in the current study. Instead, a method using HA and calcium fluoride as the starting chemicals was employed in this study [9]. To produce pure FA, solid state reactions have normally been used [21, 22], and in the current work, a solid state chemical reaction based on reference [21] has been used to prepare the FA material.

2. Materials and methods

2.1. Synthesis of HA

The method of synthesizing HA involved a metathesis reaction [11, 16]. 0.5 M calcium nitride (99.0%, Aldrich, USA) and 0.3 M di-ammonia phosphate (99.0%, Aldrich, USA) were prepared and the pH of each solution was brought to 11–12 by adding strong ammonia (28–30%, Selby, Australia). The phosphate solution was slowly added to the calcium nitride solution, resulting in the precipitation of HA. The precipitate was aged for 7 days at room temperature. It was then thoroughly washed with demineralized water and dried in an oven at 80 °C for 16 h. The resulting HA cake was ground into a fine powder using an agate mortar and pestle, and this uncalcined material is referred to as HA. Some of the HA powder was calcined at 1000 °C for 1 h in air, and this material is subsequently called calc-HA.

2.2. Synthesis of partially substituted hydroxyapatite (fHA)

The synthesis of fHA is described as follows [9]: 10 g of HA prepared by the above method was suspended in 500 ml of 0.01 M calcium fluoride (325 mesh, 99.9%, Aldrich, USA) solution. This system was equilibrated to pH 7 overnight. The pH of the solution was then decreased to 4 by slowly adding 1 M HNO_3 (68.5–69.5%, Merck, Germany). After 30 min, the pH of the solution was brought back to 7 by the addition of 1 M NaOH (99%, Merck, Germany). The cycle of pH fluctuation was repeated three times. The precipitates were filtered using a Büchner funnel with application of mild suction. The filtrate was washed three times. The resulting filter cake was dried in a fan-assisted oven overnight at 80 °C, and was then ground into powder. Finally the powder was milled by an agate miller (Siebtechnik, Germany) at a rate of 710 cycles/min for 10 min to further reduce the particle size. Some of the fHA powder was calcined in an electrical furnace at 1000 °C for 1 h in air, and the resulting powder is referred to as calc-fHA.

2.3. Preparation of FA

The FA material was prepared according to a solid state reaction [21]. The reaction temperature was adjusted in the current study in order to achieve the complete reaction. Calcium fluoride (99.9%, Aldrich, USA) and tricalcium phosphate (95%, May and Baker Ltd., UK) were mixed by an agate miller at a Ca/P ratio of 1.67. The

mixed chemicals were put into an alumina crucible and heated to 1200 °C for 2 h in an electrical furnace (Ceramic Engineering, Australia). A solid FA cake was produced, which was ground into powder using an agate mortar and pestle. The powder was then milled by an agate miller at a rate of 710 cycles/min for 10 min to further reduce the particle size.

2.4. X-ray diffraction

XRD of all powders was carried out using a Philips PW1050 X-ray diffractometer, with a cobalt target, and voltage and current settings of 40 kV and 40 mA, respectively. All samples were examined from 10° to 70° 2θ at a scanning speed of 1°/min 2θ and a step size of 0.03° 2θ. The cell references of calc-HA, calc-fHA and FA were calculated by a computer program (MDI Jade 5.0, XRD Pattern Processing, USA). Short-range patterns were obtained for the calc-HA, calc-fHA and FA specimens, using a copper target and voltage and current settings of 45 kV and 40 mA (Philips X'Pert MPD, The Netherlands). For these measurements the specimens were scanned from 31° to 35° 2θ at a scanning speed of 0.2°/min 2θ and a step size of 0.01° 2θ.

2.5. Fourier transform infra-red and FT-Raman spectroscopy

All five powders (HA, calc-HA, fHA, calc-fHA and FA) were examined by Fourier transform infra-red (FTIR: Perkin Elmer, 1600 Series FTIR, USA). 1 mg of the powdered sample was carefully mixed with 300 mg of KBr (infrared grade) and pelletized under vacuum. The pellets were analyzed in the range 4000-400 cm^{-1} at 2 cm^{-1} resolution by 16 scans. FT-Raman spectra of samples HA, fHA and FA were run on a Perkin Elmer System 2000 FT-Raman spectrometer (200 scans, 4 cm^{-1} resolution, 4000–200 cm^{-1} range) with a Nd-YAG near-infrared laser. All spectra were recorded at ambient temperature.

2.6. Bulk element analysis

Samples of 10 mg were dissolved in 1 M HCl (10 ml), diluted 1 : 100 and analyzed for calcium and phosphorus on a Spectroflame ICP-AES instrument. Standard solutions were made from KH_2PO_4, and $CaCO_3$ dissolved in hydrochloric acid. Fluoride analysis was done using a fluoride-selective electrode in citrate-hydrochloride acid buffer [23]. Samples of 10 mg were dissolved in 0.2 M HCl (20 ml) to which was added water (10 ml) and 0.2 M trisodiumcitrate (40 ml). Standard solutions were made from NaF in the same buffer system.

2.7. TEM, electron diffraction and EDX

Dilute suspensions of the HA, fHA or FA powders in deionized water were dispersed on copper TEM grids coated with a thin Formvar-carbon support film, and allowed to air-dry. The grids were examined in a transmission electron microscope (Philips CM200 TEM, Eindhoven, The Netherlands) operated at 200 kV. Single crystal and polycrystalline electron diffraction patterns were obtained from individual grains or small clusters of grains by selected-area electron diffraction. The electron lenses were normalized prior to recording each pattern to eliminate hysteresis and enhance reproducibility. The diffraction camera constant was calibrated using MoO_3 crystals with a precision of 0.49% relative error. The negatives were scanned at 300 dpi. Ring patterns were measured using the program ProcessDiffraction [24]. For spot patterns, **g**-vector distances for independent diffraction spots, and the angles between the vectors, were measured from the digital images using an image analysis program to a precision of 0.1 mm and 0.1°. These measurements were used with the program DFtools (J. Sutliffe, Lehigh University, USA) to index and quantitatively match the observed patterns to those predicted for a range of known structures for apatites and potential impurities. Best matches could then be assessed on the basis of the overall highest fit factors. Unit cell parameters and space group information for the compounds used for matching were taken from the International Center for Diffraction Data (ICDD) powder diffraction database, and are listed in Table I. The list includes potential by-products and impurities from the wet or solid state chemical reactions,

TABLE I Structures of apatite compounds and possible impurities used for matching of electron diffraction patterns. Data from the International Center for Diffraction Data powder diffraction database. Unit cell parameters (a, b, c) given in Ångstroms

No.	Chemical names and their formula	ICDD PDF No.	Crystal system	Space group	a, b	c
1	Hydroxyapatite (syn) $Ca_5(PO_4)_3OH$	09-0432	Hexagonal	$P6_3/m$ (176)	9.4180	6.8840
2	Fluorapatite (syn) $Ca_5(PO_4)_3F$	15-0876	Hexagonal	$P6_3/m$ (176)	9.3684	6.8841
3	Carbonate-hydroxylapatite (syn) $Ca_{10}(PO_4)_3(CO_3)_3(OH)_2$	19-0272	Hexagonal	$P6_3/m$ (176)	9.3090	6.9270
4	Calcium carbonate phosphate fluoride hydroxide $Ca_{10}(PO_4)_5(CO_3)(OH)F$	21-0145	Hexagonal	$P6_3/m$ (176)	9.4147	6.8663
5	Calcium fluoride carbonate phosphate hydroxide $Ca_{10}(PO_4)_5 \cdot CO_3 \cdot F_{1.5} \cdot (OH)_{0.5}$	31-0267	Hexagonal	$P6_3/m$ (176)	9.3460	6.8870
6	Calcium phosphate hydroxide (syn) $Ca_9(PO_4)_6(OH)_{1.68}$	86-1203	Hexagonal	$P6_3/m$ (176)	9.4265	6.8655
7	Whitlockite (syn) $Ca_3(PO_4)_2$	09-0169	Rhombohedral	R3c (167)	10.4290	37.3800
8	Calcium phosphate $Ca_3(PO_4)_2$	70-0364	Monoclinic ($\beta = 126.2°$)	$P2_1/a$ (14)	12.8872, 27.2840	15.2192
9	Calcium phosphate $Ca_3(PO_4)_2$	70-2065	Rhombohedral	R3c (161)	10.4391	37.3756
10	Fluorite (syn) CaF_2	35-0816	Cubic	Fm3m (225)	5.4631	5.4631
11	Calcium fluoride CaF_2	77-2096	Cubic	Fm3m (225)	5.4355	5.4355
12	Calcium oxide CaO	77-2010	Cubic	Fm3m(225)	4.8025	4.8025

including tricalcium phosphate, and several carbonate-apatite forms in which one or more of the PO_4 groups is substituted by CO_3. These forms belong to the same space group as HA and FA and have similar unit cell parameters, and could only be excluded when spectroscopic data showed an absence of the carbonate group. By minimizing the sum of the squares of the errors between calculated and observed *d*-spacings and angles, it was possible to calculate separately the optimal unit cell parameters that would best explain an observed and indexed spot pattern. These calculations were done for electron diffraction patterns that corresponded to a hexagonal apatite structure.

Elemental analysis of single grains or small clusters in the powders was carried out by energy-dispersive X-ray spectrometry (EDX) on the TEM, using a Link ISIS X-ray microanalysis system with a thin-window Si (Li) EDX spectrometer (Oxford Instruments, UK). Element concentrations and Ca : P and F : Ca ratios were calculated from the spectra after standardization for Ca and P using $Ca_3(PO_4)_2$, and for F using CaF_2. Corrections for FKα X-ray absorption in small irregular particulates are inexact, and since the particles were small the corrections were omitted to avoid overestimating the F composition. Hence the values of F : Ca measured by EDX constitute a lower limit.

3. Results

3.1. Particle morphology

TEM micrographs of the powders are shown in Fig. 1. The uncalcined HA and fHA particles (Fig 1(a) and (c)) were similar in size and morphology, typically round-ended prismatic crystals averaging about 20 × 60 nm in size. The particle lengths ranged from 20 to 120 nm. After calcination at 1000 °C for 1 h, the HA (Fig. 1(b)) and fHA particles were considerably larger and spheroidal, with an approximate diameter of 140 nm. Particles from the FA sample (Fig. 1(d)) exhibited a more plate-like and irregular morphology than the uncalcined HA and fHA particles, and the grains were about twice as large as those in the uncalcined HA and fHA powders.

3.2. X-ray diffraction

Broad range X-ray diffraction patterns (Fig. 2) from the HA and calc-HA samples were consistent with a pure HA. The patterns from fHA and calc-fHA were qualitatively similar to those of HA and calc-HA. Both HA and fHA showed broader peaks than their calcined forms, while the pattern from FA displayed sharp peaks. Traces of CaO were found in some batches of FA samples, probably resulting from the oxidation of CaF_2

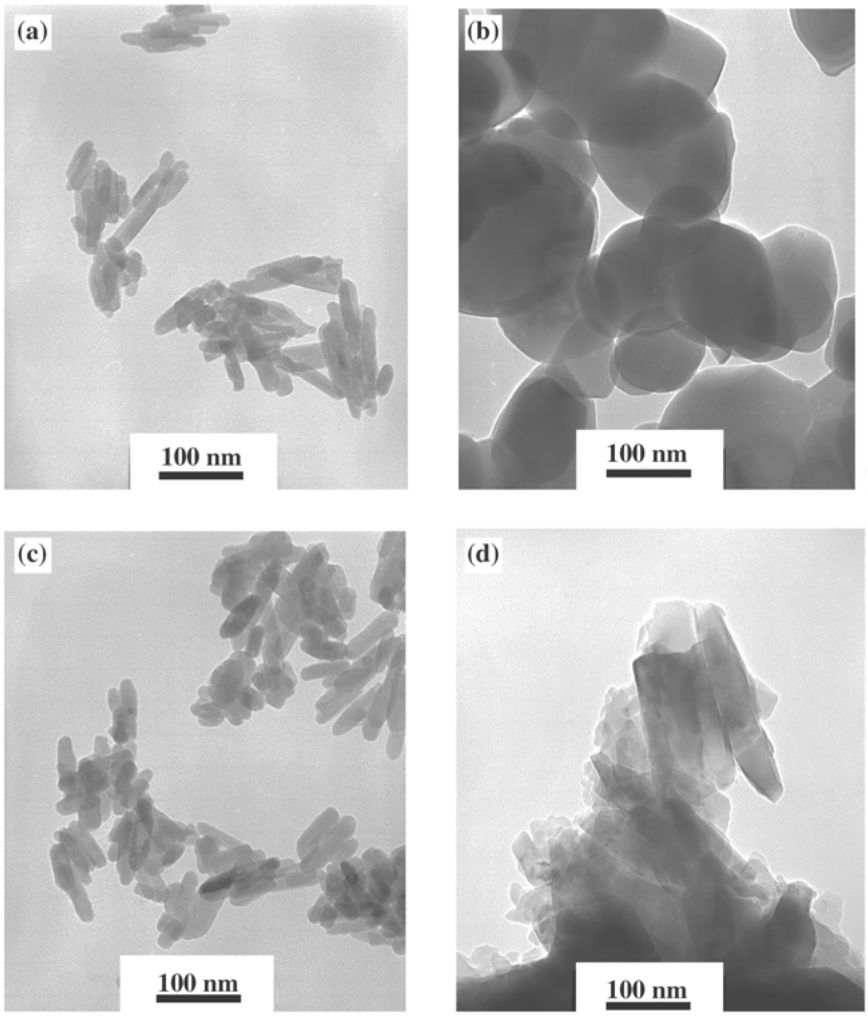

Figure 1 TEM images of (a) HA, (b) calc-HA, (c) fHA and (d) FA.

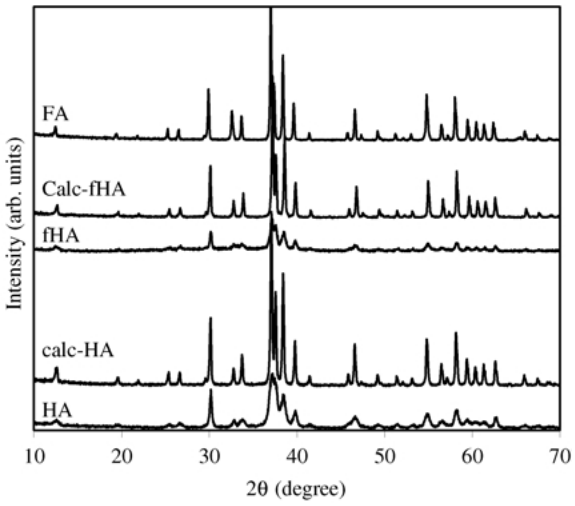

Figure 2 Broad-range XRD patterns of HA, calc-HA, fHA, calc-fHA and FA.

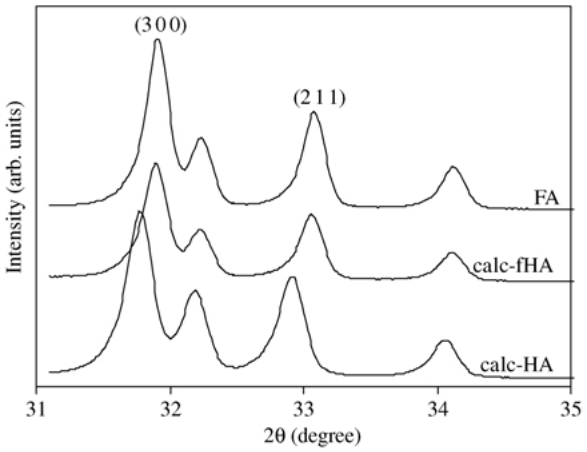

Figure 3 Short-range XRD patterns of calc-HA, calc-fHA and FA.

in air during the reaction. No tricalcium phosphate was detected by XRD in any of the five powders. However, it was not possible to distinguish a FA phase in the presence of HA from such long-range XRD patterns as in Fig. 2. Consequently short-range XRD patterns with a much slower step size were collected for the calcined samples, and these are shown in Fig. 3. It was found that the (3 0 0) reflection peak (located between 32.5° and 33.5° 2θ) of FA was shifted toward a higher 2θ relative to that from HA, while the (3 0 0) peak of fHA was intermediate between the two, but closer to that of FA. The (0 0 2) peak was not significantly changed. These shifts are reflected in the calculated cell references of calc-HA, calc-fHA and FA, which are listed in Table II. The values for fHA appear much closer to those of FA than of HA.

3.3. FTIR and FT-Raman

All five FTIR spectra of the specimens showed typical phosphate vibration modes of apatites. No HPO_4^{2-} vibration at 867 cm^{-1} was observed. However, carbonate vibrations at 875–976, 1422 and 1455 cm^{-1} were observed in both HA, fHA and calc-fHA (calculated carbonate content [25] in Table III). FTIR spectra of calc-HA, calc-fHA and FA are shown in Fig. 4. The OH stretching mode at 3570 cm^{-1} was present in sample calc-HA (as well as in HA and fHA) but absent in sample FA. From the OH vibrations in calc-fHA (3538 and 746 cm^{-1}), and on the assumption of a pure substitution of F for OH, the F-content could be estimated to be at least 75% [7, 8]. The FT-Raman spectra of the ν_3 phosphate modes of the non-calcined samples HA and fHA, as well as of FA are shown in Fig. 5. The Raman bands in sample fHA are very close to those of HA but very different from those of FA, indicating that the phosphate environment is very similar for the HA and fHA samples.

3.4. Electron diffraction

Fig. 6 shows electron diffraction patterns from the synthesized powders. Because of the very small crystallite size of the uncalcined HA and fHA, the patterns from

TABLE II Calculated hexagonal unit cell parameters *a* and *c* (in) for calc-HA, calc-fHA and FA, as determined by X-ray diffraction and electron diffraction. Errors are ± standard error of the mean, with the number of measurements in parentheses

Sample	XRD		Electron diffraction	
	a	*c*	*a*	*c*
Calc-HA	9.4155	6.881	9.402 ± 0.020 (8)	6.914 ± 0.067 (7)
Calc-fHA	9.3769	6.885	9.398 ± 0.033 (11)	6.875 ± 0.062 (9)
FA	9.3716	6.884	9.358 ± 0.023 (10)	6.841 ± 0.058 (9)

TABLE III Elemental ratios of Ca : P and F : Ca, and the carbonate and fluoride content in the five apatite powders as measured by different methods. The means for F : Ca by EDX represent minimum values; *n* = number of analyses

Method	Measurement	HA	Calc-HA	fHA	Calc-fHA	FA
ICP-AES	Ca : P ratio	1.64	1.63	1.63	1.65	1.70
F-electrode	F : Ca ratio	—	—	0.138	0.161	0.179
FTIR	% CO_3	1.7%	None	2.4%	Trace	None
EDX	Ca : P ratio					
	Mean:	1.632	1.592	1.678	1.614	1.694
	Range:	1.523–1.982	1.531–1.661	1.622–1.769	1.546–1.712	1.531–1.964
	n:	10	10	11	11	11
EDX	F : Ca ratio (means)	—	—	0.081	0.0	0.149

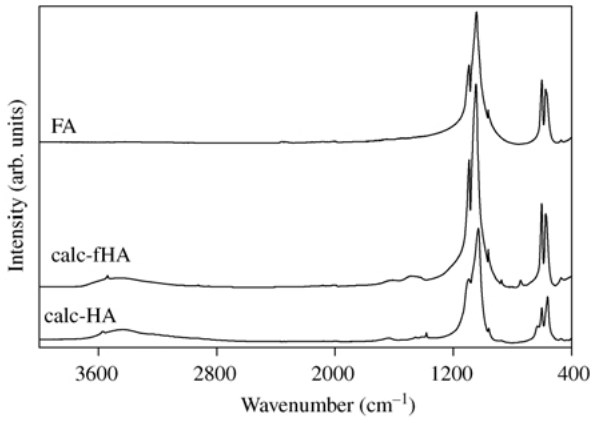

Figure 4 FTIR spectra of calc-HA, calc-fHA and FA.

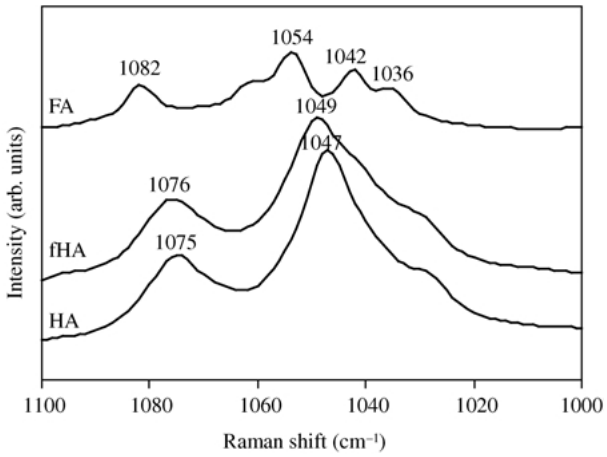

Figure 5 FT-Raman spectra of HA, fHA and FA.

these samples were mainly polycrystalline ring patterns (Fig. 6(a) and (b)). In HA, the strongest ring includes contributions by the 1 1 $\bar{2}$ 2 and 3 0 $\bar{3}$ 0 planes at 0.278 and 0.281 nm respectively, while in FA, these *d*-spacings are nearly identical at 0.277 and 0.280 nm. The *d*-spacings in the HA patterns were consistent with HA, whereas spacings in the fHA patterns variously corresponded to those from either FA or HA. However, it was not possible to discriminate between these two apatites from such ring patterns.

Predominantly single crystal spot patterns could be obtained from the FA and calcined HA and fHA samples. For the calc-HA sample, most (6 out of 10) of the patterns best matched the HA reference (PDF file 09-0432 in Table I), and only one pattern indicated tricalcium phosphate (PDF 70-0364). A major zone-axis pattern corresponding to HA is shown in Fig. 6(c). The remaining patterns from calc-HA appeared to correspond slightly better to a calcium phosphate hydroxide (PDF 86-1203, structurally very similar to HA), though the differences in the fit factors as compared to HA were only about 2%. For the calc-fHA sample, the majority of patterns fitted either the HA (2/12) or the calcium phosphate hydroxide form (7/12) (Fig. 6(d)). Only two of the patterns best fitted the FA reference (PDF 15-0876) (Fig. 6(e)), while one pattern suggested a tricalcium phosphate impurity.

In contrast to the calc-fHA sample, most (10/14) of the patterns from the FA sample best matched FA, of which the [0 0 0 1] pattern in Fig. 6(f) is an example. Only two patterns were closer to the HA, and two indicated tricalcium phosphate. Other possible impurities such as CaO and CaF_2 could not be matched to any of the patterns obtained from the samples. The average unit cell parameters calculated from the electron diffraction patterns of individual grains are summarized in Table II, in comparison to the refined cell parameters from XRD. Since each measurement is subject to some instrumental error, and the patterns are sensitive to sample effects such as grain orientation and internal strain, some variability in the results is expected and this is reflected in the errors observed. In comparison, the XRD results were obtained from peak fits from a single pattern. However, the unit cell parameters obtained by electron diffraction were consistent with the XRD values within the experimental error.

3.5. Elemental analyses

The results of measurements of elemental composition and ratios by the different methods are summarized in Table III. The bulk Ca/P ratios determined by ICP-AES were just below the value of 1.667 expected for a pure HA or FA phase. Measurements of fluoride content using a F-selective electrode indicated a higher F/Ca ratio in calc-fHA compared to fHA, but the ratio closest to that for pure FA was measured in the FA sample. Some carbonate was detected by FTIR in HA and fHA, with traces remaining in the calcined fHA. However, no CO_3 was detected in the calcined HA and the solid reaction FA samples.

Energy-dispersive X-ray spectra from the HA and FA samples are compared with a spectrum from a tricalcium phosphate standard in Fig. 7. The carbon peak derives from the substrate film. Ca/P ratios were calculated from EDX spectra of individual grains or small clusters, and are given in Table III as mean values together with the range. The range of individual values by EDX encompasses the ratios in the bulk material determined by ICP. The mean F/Ca ratios measured by EDX are also shown in Table III. These values represent a lower limit, but indicate a low F content in fHA and a relatively high F content in FA. Curiously no significant F content could be detected in the calc-fHA sample. Several impurities were also identified by EDX, the results for which are not included in the reported means. In the fHA sample, some impurities showed values of Ca/P ratio of about 2.9, and F/Ca of about 0.45, far in excess of those expected for FA of 1.67 and 0.2, respectively. Such high Ca/P ratios may be found in carbonate-apatites, or in apatites containing additional calcium as calcium oxide or hydroxide impurities. The high F/Ca indicated F-rich impurities, or a mixture of CaF_2 and other calcium oxides, hydroxides or phosphates. In the FA sample, the presence of some small grains of mainly CaO and CaF_2 could be directly identified from their EDX spectra.

4. Discussion

The morphology of the particles in sample HA was similar to that obtained by Jha *et al*. [10] and Wei *et al*. [11], though the particles reported by Wei *et al*. were smaller probably due to the lower reaction temperature

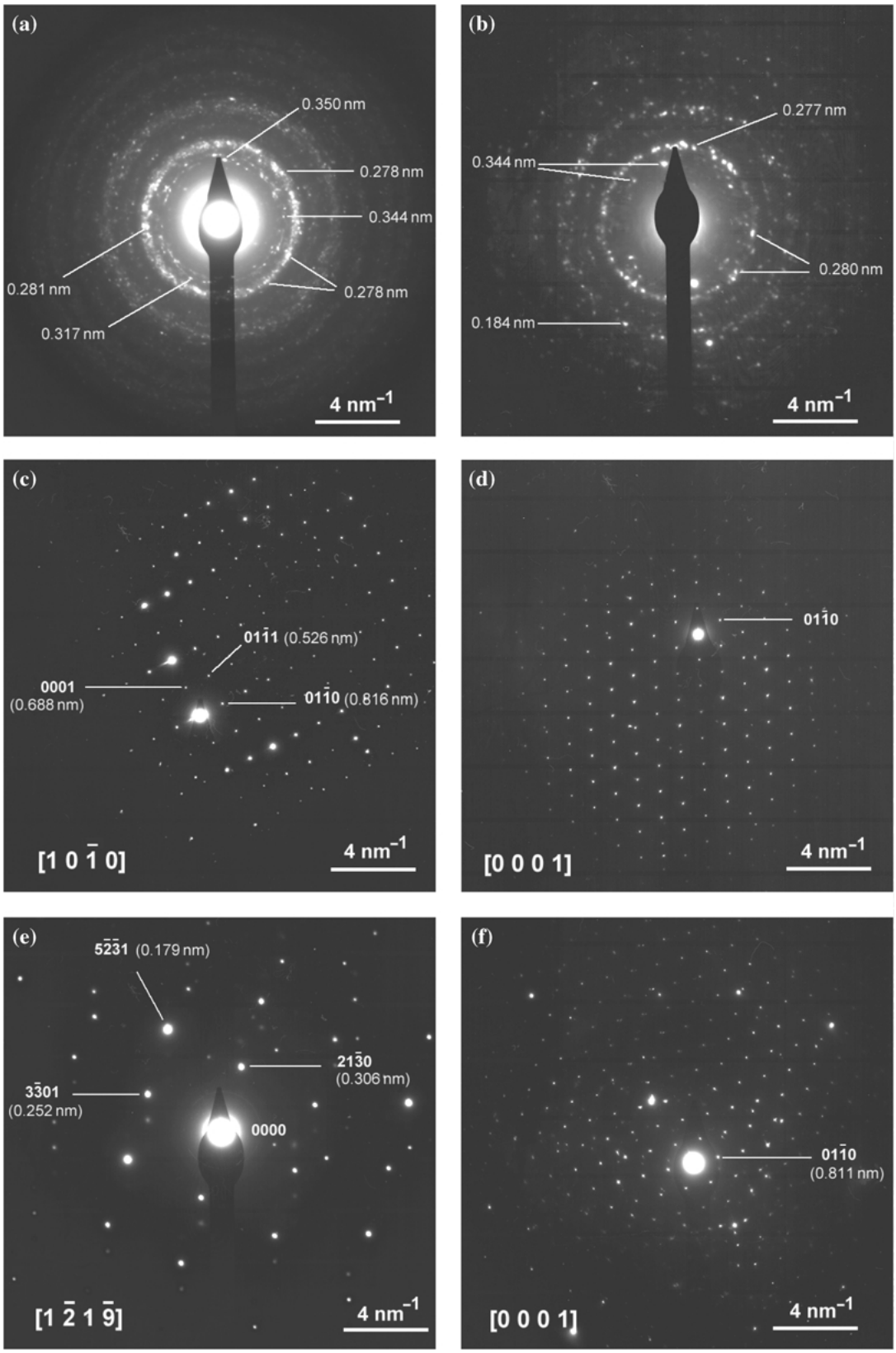

Figure 6 Polycrystalline electron diffraction patterns for (a) HA and (b) fHA, and single crystal patterns from (c) calc-HA (matches HA), and (d) calc-fHA (matches calcium phosphate hydroxide); (e) and (f) are FA patterns from samples calc-fHA and FA, respectively.

used [11]. The fluoride substitution reaction resulted in no significant morphological change in the particles, presumably since fHA was directly derived from HA. The substitution was a very gentle process, conducted by fluctuating the pH of the solution at room temperature. The production of FA involved a solid reaction at a high temperature, and yielded relatively larger crystals than the uncalcined HA and fHA. Calcination of the HA and fHA samples produced a marked change in size and shape, leading to much larger spheroidal crystals. The polycrystalline electron diffraction patterns from calcined HA and fHA (Fig. 6) generally showed sharper rings than the uncalcined material, indicating increased crystallinity following calcination, in agreement with the XRD observations. FTIR results also showed that calcination resulted in the removal of virtually all

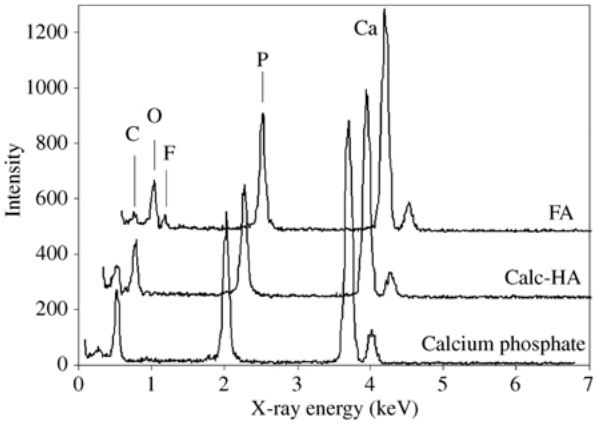

Figure 7 Energy-dispersive X-ray spectra from the FA and calcined HA samples, in comparison to tricalcium phosphate. The spectra are offset by 0.25 keV for display.

residual CO_3 groups in the HA and fHA samples (Table III).

The long-range XRD patterns (Fig. 2) indicated that pure apatite was formed in all five samples, and traces of other calcium phosphate impurities were not detected by this technique. In the short range XRD (Fig. 3), the (3 0 0) reflection peak of calc-fHA was shifted to a higher angle towards FA, an observation that was also reported by Okazaki *et al*. [20]. In the present study, the (3 0 0) peak of calc-fHA was closer to that of FA than to that of calc-HA, indicating specifically that the unit cell *a*-axis parameter of calc-fHA must be closer to that of FA. This is reflected in the refined unit cell parameters from XRD in Table II. The *a* parameter for FA (0.9372 nm) was in turn only slightly higher than the reference value for FA of 0.9368 nm. Thus the XRD observations suggest that calc-fHA possesses a structure intermediate between HA and FA but closer to the FA form. This in turn suggests that replacement of most lattice OH with F must have taken place.

The bulk fluoride content in the fHA samples fHA and calc-fHA (obtained from fluoride selective electrode measurements, Table III) was found to be 65% and 78%, respectively. The information extracted from the FTIR and FT-Raman spectra was that the OH and phosphate environments of fHA were very close to that of HA (i.e. the OH vibration was unchanged in the FTIR spectra and the phosphate modes were similar in the FT-Raman spectra). In other words, the spectra of fHA indicate that there is $< 5\%$ fluoride present. In contrast, calc-fHA had shifted OH vibrations from which a fluoride content could be estimated to be 75% or more, and this is in agreement with F-selective electrode analysis for calc-fHA. Thus the vibrational spectroscopic information agrees with the bulk analysis for calc-fHA, but not for fHA. Further studies into this disagreement are currently being undertaken [26] and results suggest that care has to be taken when interpreting FTIR and FT-Raman spectra of partly fHA.

The main HA and FA phases are difficult to distinguish by X-ray diffraction, except by close examination of the (3 0 0) peak. Furthermore, some low level impurities may not be detected by XRD, especially if their patterns are overlapped by stronger patterns. Therefore electron diffraction measurements were carried out in an attempt to identify individual constituent crystalline phases in the synthesized powders, including possible impurities. Electron diffraction was used as a complementary technique to bulk characterization by XRD, but since the measurements are specific to individual selected grains or small areas, it is difficult to extrapolate the results to the bulk material. Quantitative matching of electron diffraction spot patterns showed that it was possible to discriminate reasonably well between the HA and FA forms. These forms effectively correspond to end structures with 0% and 100% substitution of F for OH. However, there are many other related apatite structures, including the carbonate apatites in Table I, where the differences between unit cell dimensions are smaller. Such structures are difficult if not impossible to distinguish by selected area diffraction because of residual instrumental and measurement errors. On the other hand, potential impurities with non-hexagonal symmetry could be relatively easily identified by quantitative matching. A few patterns indicated monoclinic tricalcium phosphate (PDF 70-0364), but other calcium phosphates, fluorides or oxides were not identified by electron diffraction, nor were they apparent in the XRD patterns.

The electron diffraction ring patterns from uncalcined HA and fHA indicated only that the patterns were consistent with the main apatites. However, from measurements of the spot patterns from the FA and calcined HA and fHA samples, it was possible to confirm that calc-HA was predominantly HA, while FA was predominantly FA. For the calc-fHA sample, the matching was more inconsistent, in that the patterns variously fitted either FA, HA, or a calcium phosphate hydroxide. This variability is also reflected in the larger error in the calculated average cell *a* parameter for calc-fHA in Table II. Many of the patterns from calc-HA and calc-fHA appeared to give a marginally better fit to a calcium phosphate hydroxide form (PDF 86-1203, Table I) as compared to the reference HA. This material, effectively a calcium-deficient HA (formula $Ca_9(PO_4)_6(OH)_{1.68}$), is very similar to HA but has a Ca/P ratio of only 1.5. The short-range XRD results (Fig. 3 and Table II) suggest that calc-fHA has a structure intermediate between the HA and FA forms. However, no structures for partially F-substituted carbonate-free apatites are recorded in the ICDD database. Given the close similarities between the HA, FA, calcium-deficient HA, and carbonated apatites (Table I), the fHA structure may lie between these forms. FTIR and Raman spectroscopy indicated that carbonate was incorporated at trace levels into the lattice structure of calc-fHA, but unequivocal matching of diffraction patterns to the carbonate apatite forms was not obtained. We interpret the variability in the matching for calc-fHA patterns as indicative of the presence of intermediate structures together with some HA and FA, making the sample probably more heterogeneous than calc-HA or FA. Given the difficulties of distinguishing very similar structures by quantitative matching, it is not clear whether the apparent fits to the calcium phosphate hydroxide indicate that this compound is actually present, or simply point to the presence of some intermediate material of similar structure. However, if some calcium phosphate hydrox-

ide were present, it would at least partly explain the observed Ca/P ratios below the predicted value of 1.667 for pure HA or FA (Table III). It is unlikely that the reduced ratios are simply due to the presence of impurities such as tricalcium phosphate. Although some tricalcium phosphate was indicated by electron diffraction of individual grains, the overall weight fraction must have been small (< 1–2%) or this impurity would have been evident in the XRD patterns.

For measurements of element composition, the ICP, F-electrode and FTIR analyses represent an overall measurement of the bulk content, while the EDX analyses performed on the TEM are of individual grains or small clusters. The value of EDX analysis is the capability of identifying specific constituents and impurities in single particles, but again it is difficult to extrapolate the results to the bulk case. Nevertheless, the Ca/P ratios measured by ICP and EDX are consistent in that the ICP values fall within the range of values measured by EDX. Individual Ca/P ratios by EDX lower than 1.667 may result from the presence of small amounts of calcium phosphate impurity, or possibly calcium phosphate hydroxide, within the small area of analysis. Ca/P ratios higher than 1.667 can arise from the local presence of carbonated apatite compounds (for which Ca/P can be as high as 3.33, e.g. PDF 19-0272 in Table I) or impurities such as CaO or CaF_2. Although not evident by XRD or electron diffraction, the presence of small amounts of these impurities could be confirmed from EDX spectra of single grains in the FA sample (Section 3.5). Some spectra from the fHA sample also showed very high levels of Ca or F relative to P, far in excess of those expected from the main apatites, indicating the presence of Ca-rich or F-rich impurities.

In pure FA the F/Ca ratio is 0.2. The ratios measured by F-electrode and EDX in fHA, calc-fHA and FA were less than this, but highest in the FA material (Table III). The F/Ca ratios determined by EDX, though minimum values, were considerably less than those measured by the F-electrode, and curiously no significant fluorine was detected in the calc-fHA sample. The low ratios observed in fHA by EDX may be the result of electron-beam induced mass loss of fluorine in the TEM, as this element is known to be particularly volatile and electron energies were high (200 keV). However, F was much better retained in the FA sample under virtually identical analytical conditions, suggesting that there may have been some subtle differences in the way F was incorporated into the material between the calc-fHA and FA samples.

By examining individual grains of the synthesized apatite powders in the TEM it has been possible to obtain further information about the apatite and non-apatite phases (i.e. impurities) present. Some specific impurities have been identified although their levels in the samples must have been low. Such detailed information cannot be obtained from the bulk techniques used (XRD, ICP, FTIR and FT-Raman) when the overall sample purity is high ($> 98\%$). Even when the bulk results do not perfectly match the standard compounds, it can be difficult from the bulk data to establish the identity of possible impurities present. Thus a combination of macro and microtechniques has proved successful in characterizing the synthesized powders in terms of morphology, crystal structure and element and phase composition.

5. Conclusions

Synthetized apatite powders have been characterized on a macroscopic level by XRD, FTIR, FT-Raman and chemical analysis, while TEM, EDX and electron diffraction have provided detailed information at the microscopic (individual grain) level. These complementary techniques have shown that the HA sample prepared in solution was nearly pure HA, while the FA sample prepared by a solid reaction was nearly pure FA. Only low levels of specific impurities were detected. Calcination of the HA and F-substituted HA (fHA) powders resulted in increased grain size and crystallinity, as well as loss of residual carbonate groups from the samples. The structure of the fHA sample appeared to be intermediate between the HA and FA forms, and incorporation of F into the lattice structure was incomplete. The solid reaction process yielded the most phase pure FA.

Acknowledgments

The authors would like to thank Mr T. Raftery, X-Ray Analysis Facility, QUT, for his expert assistance in the X-ray diffraction analyses. Dr L. Grøndahl acknowledges the QUT postdoctoral research fellowship.

References

1. R. Z. LEGEROS and J. P. LEGEROS, in ''An Introduction to Bioceramics'', edited by L. L. Hench and J. Wilson (World Scientific, Singapore, 1993).
2. M. OKAZAKI, Y. MIAKE, H. TOHDA, T. YANAGISAWA, T. MATSUMOTO and J. TAKAHASHI, *Biomater.* **20** (1999) 1421.
3. J. C. ELLIOTT, in ''Studies in Inorganic Chemistry'', Vol. 18 (Elsevier, Amsterdam, 1994).
4. G. PENEL, G. LEORY, C. REY, B. SOMBRET, J. P. HUVENNE and E. BRES, *J. Mater. Sci. Mater. Med.* **8** (1997) 271.
5. C. B. BADDIEL and E. E. BERRY, *Spectrochemica Acta* **22** (1966) 1407.
6. Y. LIU, P. COMODI and P. SASSI, *N. Jb. Miner. Abh.* **174** (1998) 211.
7. F. FREUND and R. M. KNOBEL, *J. Chem. Soc., Dalton Trans.* (1977) 1136.
8. A. BAUMER, M. GANTEAUME and W. E. KLEE, *Bull. Mineral.* **108** (1985) 145.
9. M. BRAUN, P. HARTMANN and C. JANA, *J. Mater. Sci. Mater. Med.* **6** (1995) 150.
10. L. J. JHA, S. M. BEST, J. C. KNOWLES, I. REHMAN, J. D. SANTOS and W. BONFIELD, *ibid.* **8** (1997) 185.
11. M. WEI, A. J. RUYS, B. K. MILTHORPE and C. C. SORRELL, *J. Biomed. Mater. Res.* **45** (1999) 11.
12. H.-J. KLEEBE, E. F. BRES, D. BERNACHE-ASSOLANT and G. ZIEGLER, *J. Am. Ceram. Soc.* **80** (1997) 37.
13. H. JI and P. M. MARQUIS, *J. Mater. Sci. Letters* **10** (1991) 132.
14. E. I. SUVOROVA, F. CHRISTENSSON, H. E. LUNDAGER MADSEN and A. A. CHERNOV, *J. Cryst. Growth* **186** (1998) 262.
15. E. I. SUVOROVA and P. A. BUFFAT, *J. Microsc.* **196** (1999) 46.
16. M. JARCHO, C. H. BOLEN, M. B. THOMAS, J. BOICK, J. F. KAY and R. H. DOREMUS, *J. Mater. Sci.* **11** (1976) 2027.
17. M. HIRANO, H. TAKEUCHI and M. ONO, in ''Sintering'87 Volume 2, Proc. of the International Institute for the Science of Sintering Symposium'', edited by S. Somiya, M. Shimada, M. Yoshimura and R. Watanabe (Elsevier, Amsterdam, Holland, 1987).

18. T. FUTAGAMI and T. OKAMOTO, *J. Ceram. Soc. Jap.* **95** (1987) 775.
19. E. D. EANES and A. W. HAILER, *Calcif. Tissue Int.* **63** (1998) 250.
20. M. OKAZAKI, H. TOHDA, T. YANAGISAWA, M. TAIRA and J. TAKAHASHI, *Biomater.* **19** (1998) 919.
21. A. TRAVERIA-CROS, M. CUEVAS-DIARTE, F. PLANA-LIEVAT and M. FONT-ALTABA, *Acta Geol. Hisp.* **15** (1980) 15.
22. R. FABIAN, I. KOTSIS, P. ZIMANY and P. HALMOS, *Talanta* **46** (1998) 1273.
23. E. J. DUFF and J. L. STUART, *Anal. Chem. Acta.* **52** (1970) 155.
24. J. L. LABAR, in ''Proc. of EUREM 12, Volume III'', edited by L. Frank and F. Ciampor (Brno, Hungary, 2000).
25. J. D. B. FEATHERSTONE, S. PEARSON and R. Z. LEGEROS, *Caries Res.* **18** (1984) 63.
26. L. GRØNDAHL, L. RINTOUL, M. WEI, E. WENTRUP-BYRNE and J. H. EVANS. Work in progress.

Received 19 February
and accepted 20 August 2002